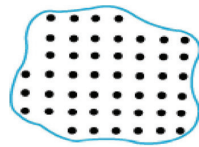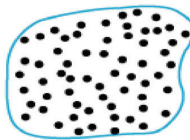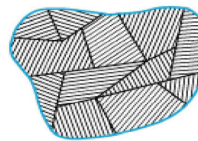**FIGURE 2.1**

Classification of materials as crystalline (a), amorphous (b), and polycrystalline (c). (Drawing by Mr. Chengwu Deng.)

(a) Crystalline   (b) Amorphous   (c) Polycrystalline

FIGURE 2.2

Any crystal lattice can be simplified to a three-dimensional array of periodically located points in space. Such a periodic array, specifying how the repeated units of a crystal are arranged, is called a *Bravais lattice*. A real crystal is made up of a basis and a lattice. (Drawing by Mr. Chengwu Deng.)
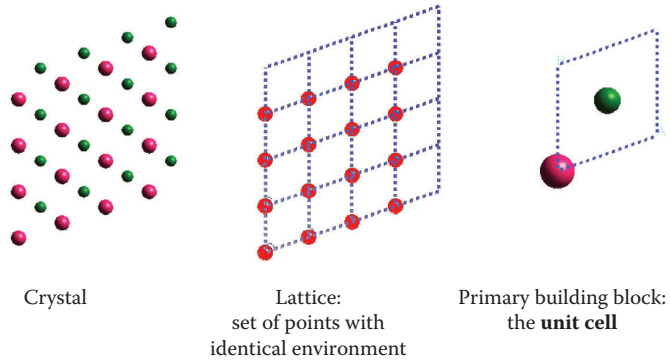

Crystal

Lattice:
set of points with
identical environment

Primary building block:
the **unit cell**

FIGURE 2.3

The simplest unit cell belongs to a cubic lattice, which is further divided into: simple cubic (SC), face-centered cubic (FCC), and body-centered cubic (BCC).

1. Simple cubic (SC)

Conventional cell = primitive cell

$\mathbf{a}_1 = \mathbf{a}_2 = \mathbf{a}_3$
$\mathbf{a}_1 \perp \mathbf{a}_2 \perp \mathbf{a}_3$

$\mathbf{a}_3$
$\mathbf{a}_2$
$\mathbf{a}_1$

Add one atom at the center of the cubic

Add one atom at the center of each face

2. Body-centered cubic (BCC)

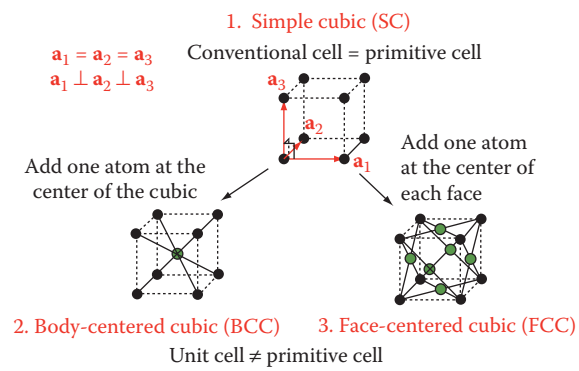3. Face-centered cubic (FCC)

Unit cell ≠ primitive cell

FIGURE 2.4

Conventional unit cells for the 14 Bravais lattices arranged according to the 7 crystal systems. P means lattice points on corners only, C means lattice points on corners as well as centered on faces, F means lattice points on corners as well as in the centers of all faces, and lattice points on corners as well as in the center of the unit cell body are indicated by I.
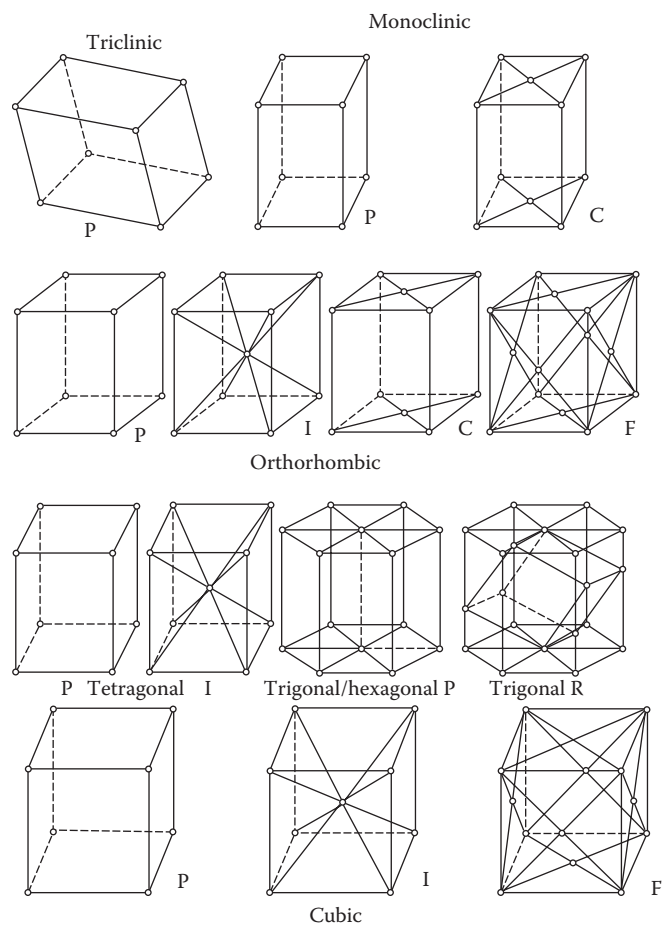
FIGURE 2.5

Wigner-Seitz primitive cells for two types of simple 2D lattices.
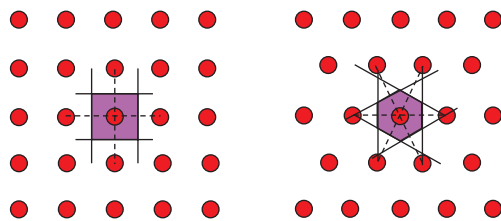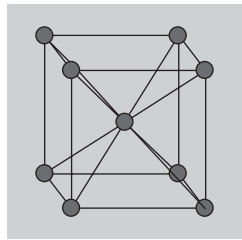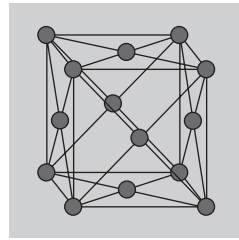
FIGURE 2.6

Conventional unit cells, primitive unit cells, and Wigner-Seitz primitive cells for BCC and FCC lattices. The BCC Wigner-Seitz unit cell is a truncated octahedron. The FCC Wigner-Seitz primitive unit cell is a rhombic dodecahedron.
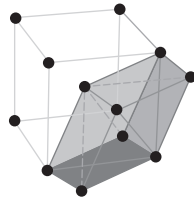
Body-centered cubic lattice (BCC)   Face-centered cubic lattice (FCC)
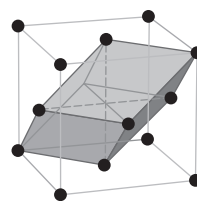

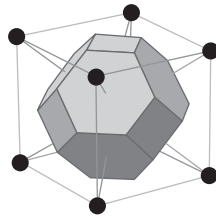
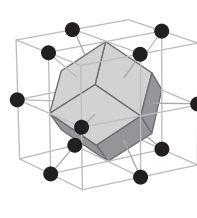Conventional cell: 2 atoms/cell   Conventional cell: 4 atoms/cell

Primitive unit cell: 1 atom/cell   Primitive unit cell: 1 atom/cell

Wigner-Seitz primitive
cell: 1 atom/cell

Wigner-Seitz primitive
cell: 1 atom/cell

FIGURE 2.7

The drawing on the left (a) is crystal-like and can be carried into itself by a translation that is not possible in the figure on the right (b). The latter is missing a translation vector and is not crystal-like.
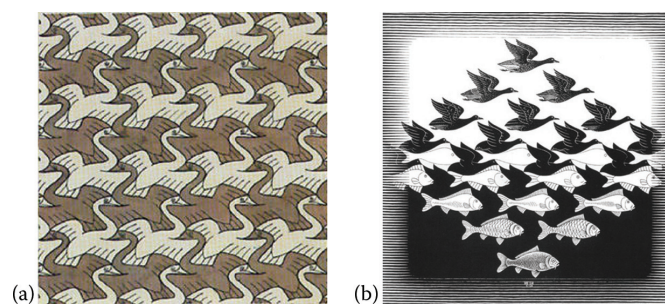

(a)   (b)

FIGURE 2.8

Point symmetry operations: (a) rotation, (b) reflection, and (c) a compound symmetry operation: inversion. The latter is made up of a rotation of π followed by reflection in a plane normal to the rotation axis. This is also called inversion through a point (i). The symbol for the inversion axis is $\bar{1}$.
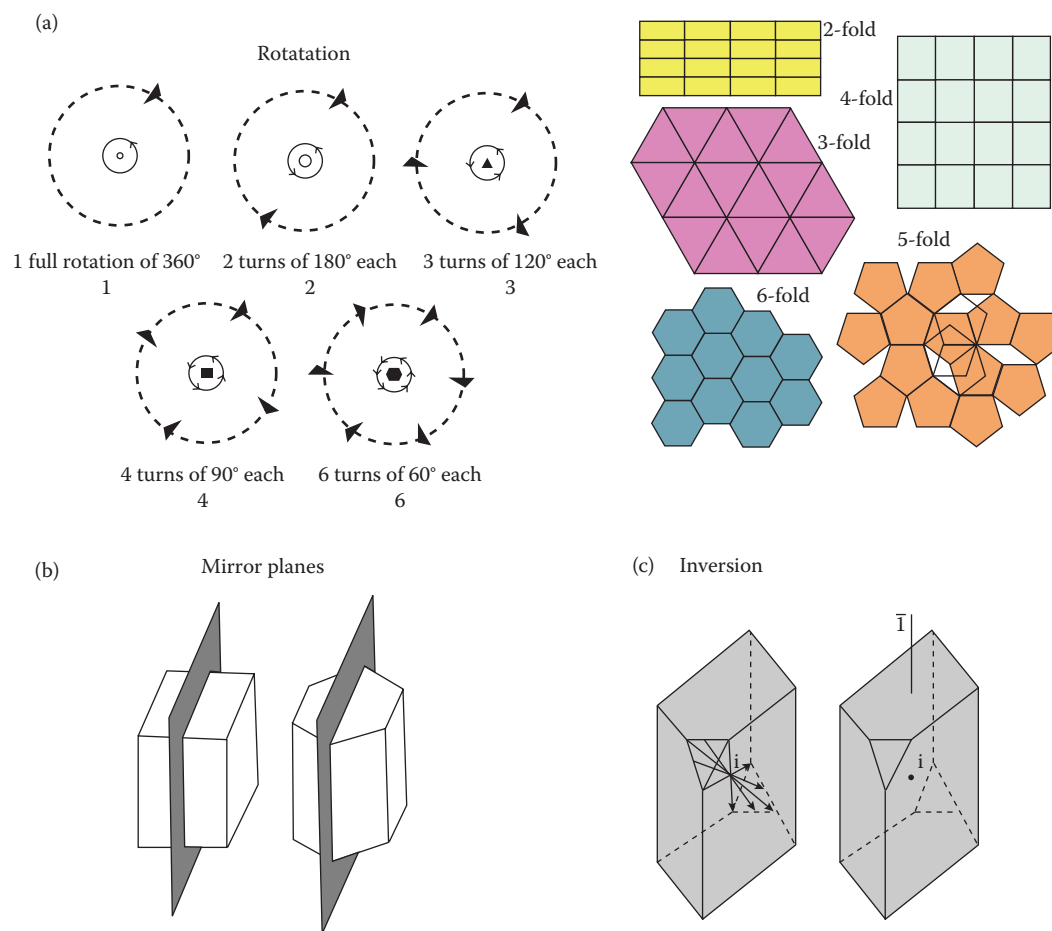
(a)

Rotatation

1 full rotation of 360°
1

2 turns of 180° each
2

3 turns of 120° each
3

4 turns of 90° each
4

6 turns of 60° each
6

2-fold

4-fold

3-fold

5-fold

6-fold

(b)   Mirror planes

(c)   Inversion

$\bar{1}$

i

i

FIGURE 2.9

Ice crystals. No pentagons are found in ice crystal stacking.

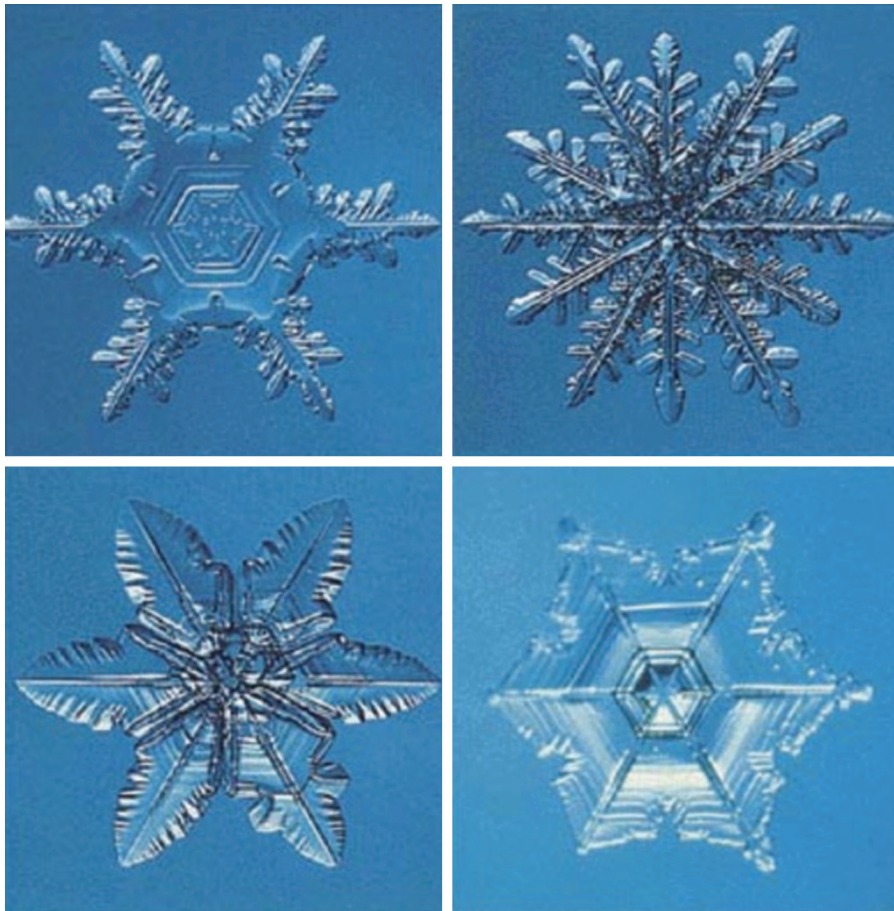## FIGURE 2.10

(A) In the pyroelectric crystal $BaTiO_3$, **P** changes with temperature only when the material is in its tetragonal state. Pyroelectricity only occurs in a crystal lacking an inversion center. This is clear from (B) (a). In cubic $BaTiO_3$ the oxygen ions are at face centers; Ba^{2+} ions are at cube corners; and Ti^{4+} is at cube center. (B) (b) in tetragonal $BaTiO_3$, the Ti^{4+} is off-center, and the unit cell has a net polarization. (Drawing by Mr. Chengwu Deng.)
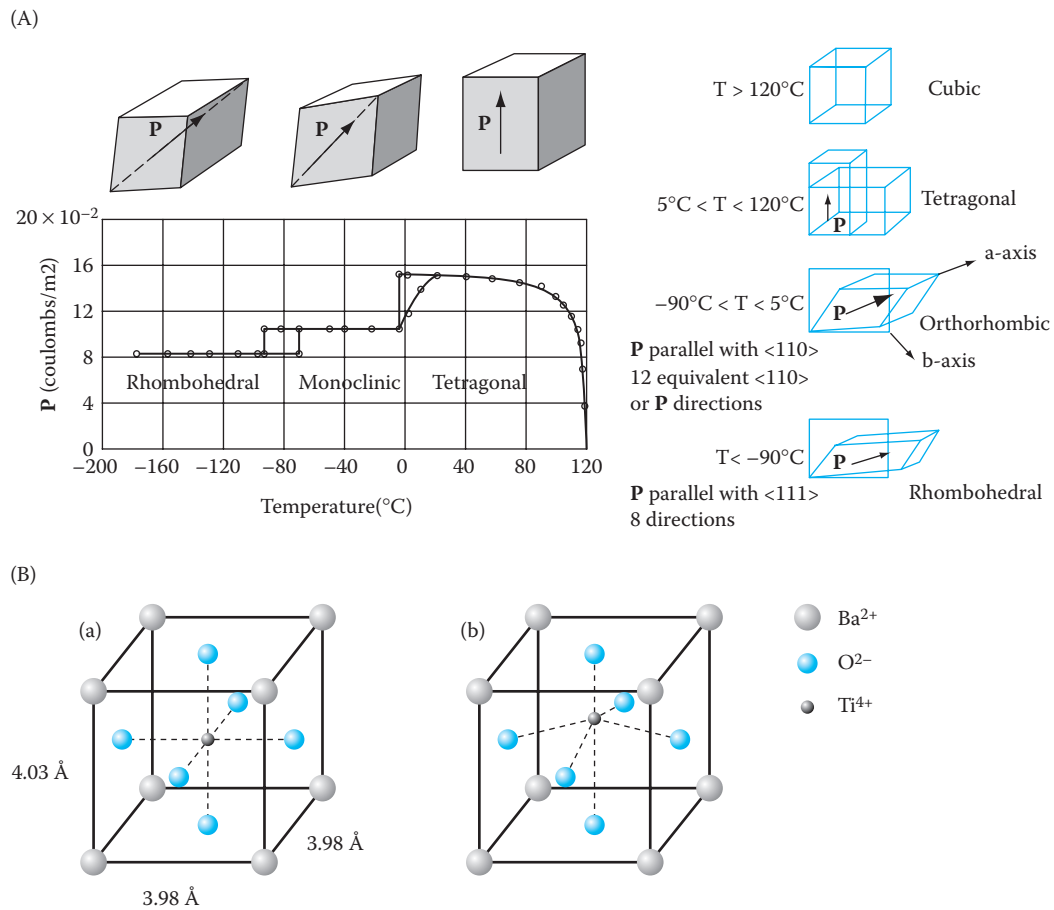
FIGURE 2.11

Example of a screw axis and a glide plane. (a) N-fold screw axes C: a combination of a rotation of $360°/n$ around C and a translation by an integer of C/n. (b) Glide plane: a translation parallel to the glide plane g by $a/2$.
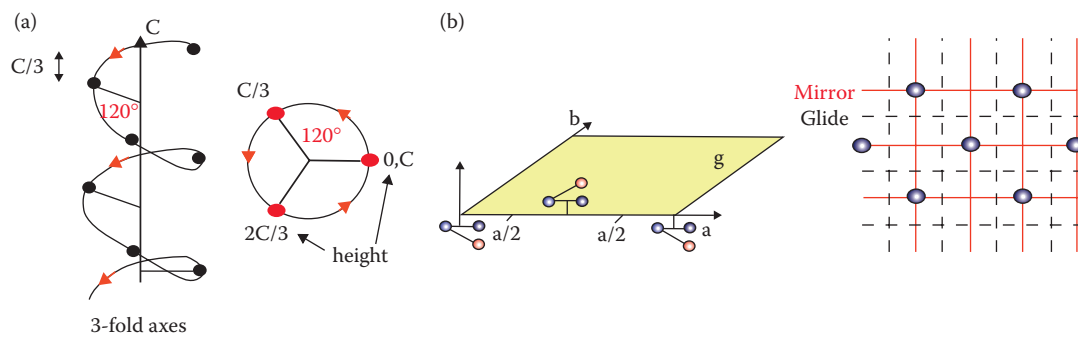
FIGURE 2.12

Miller indices for planes and directions in an SC cubic crystal. Shaded planes are from left to right (100), (110), and (111). (Drawing by Mr. Chengwu Deng.)
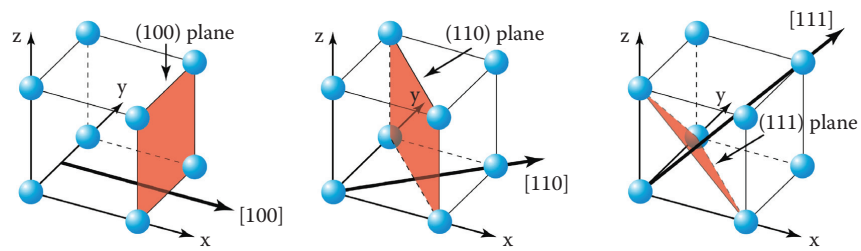
FIGURE 2.13

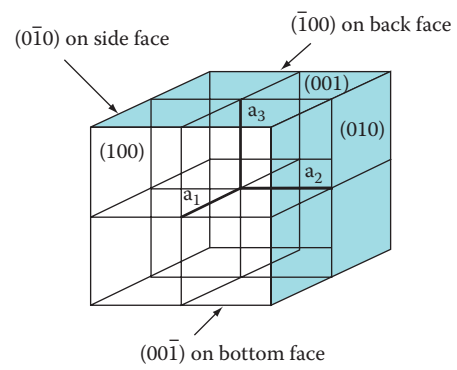Miller indices for the planes of the {100} family of planes.

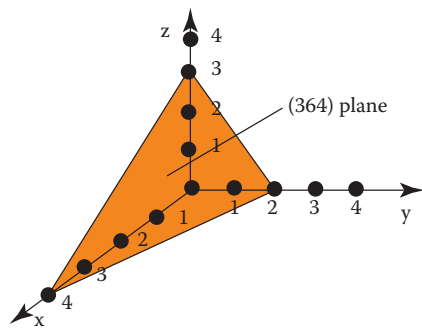**FIGURE 2.14**

The (364) plane in a SC cubic lattice.

FIGURE 2.15

(a) For periodic signals a discrete sum of sines/cosines of different frequencies is multiplied by a different weighing coefficient in a so-called Fourier series (FS). (b) For nonperiodic functions, one needs a continuous set of frequencies so the integral of sines/cosines is multiplied by a weighting function in a so-called Fourier transform (FT).
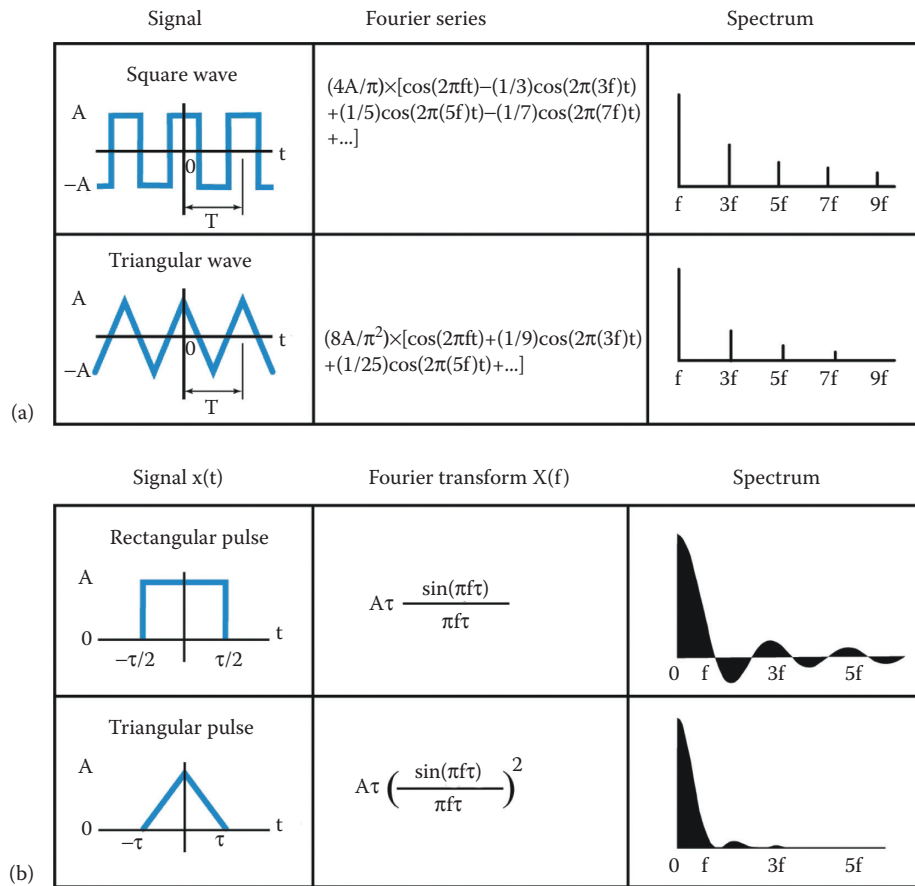
Signal	Fourier series	Spectrum
Square wave	$(4A/\pi)\times[\cos(2\pi ft)-(1/3)\cos(2\pi(3f)t)$ $+(1/5)\cos(2\pi(5f)t)-(1/7)\cos(2\pi(7f)t)$ $+...]$	
Triangular wave	$(8A/\pi^2)\times[\cos(2\pi ft)+(1/9)\cos(2\pi(3f)t)$ $+(1/25)\cos(2\pi(5f)t)+...]$	

(a)

Signal x(t)	Fourier transform X(f)	Spectrum
Rectangular pulse	$A\tau \dfrac{\sin(\pi f\tau)}{\pi f\tau}$	
Triangular pulse	$A\tau \left(\dfrac{\sin(\pi f\tau)}{\pi f\tau}\right)^2$	

(b)

FIGURE 2.16

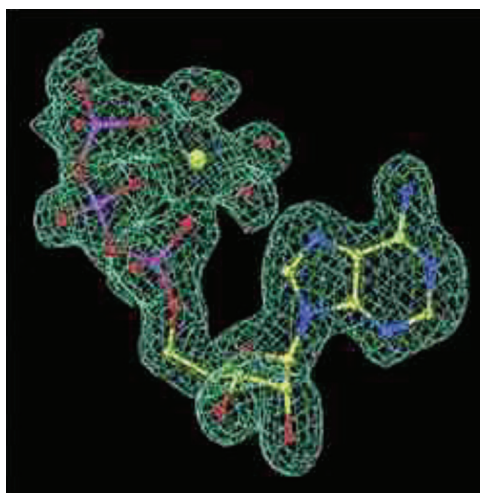Electron density map of adenosine triphosphate (ATP).

FIGURE 2.17

With x-rays, we can detect diffraction from molecules, but we have to use a computer to reassemble the electron density/molecular structure image.
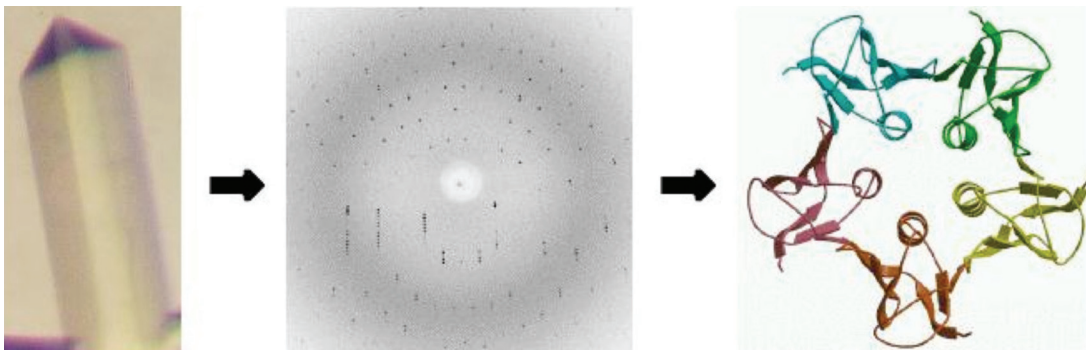
FIGURE 2.18
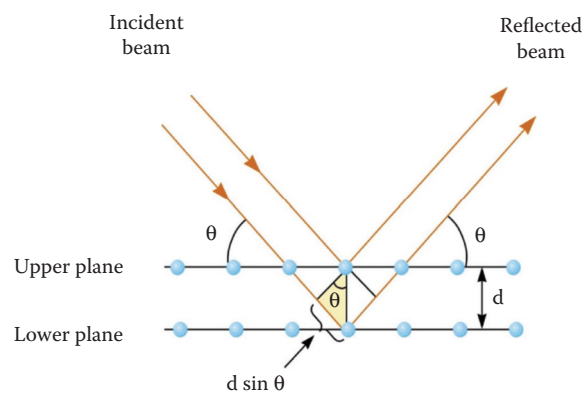
Schematic used to derive the Bragg equation.

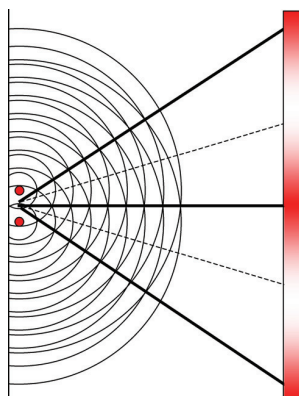**FIGURE 2.19**

Two scattering atoms act as coherent secondary sources.

FIGURE 2.20

Scattering of an incident x-ray beam (incident direction is $\mathbf{k}_0$) by a row of identical atoms with lattice spacing $\mathbf{a}_1$. The scattered beam is specified by the direction $\mathbf{k}$. The path difference $A_1B - A_2C$ must equal $e\lambda$, with $e = 0,1,2,3,....$ (Drawing by Mr. Chengwu Deng.)
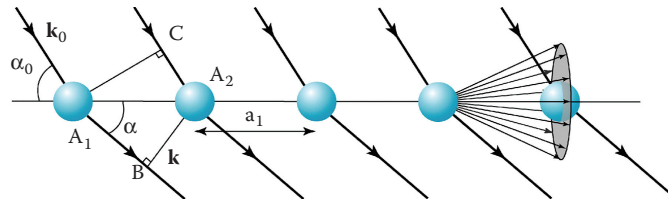
FIGURE 2.21

Each Laue condition produces a cone of allowed rays. In a plane array the entire plane scatters in phase in two directions. These two directions are along the intersection of the two cones. (Drawing by Mr. Chengwu Deng.)
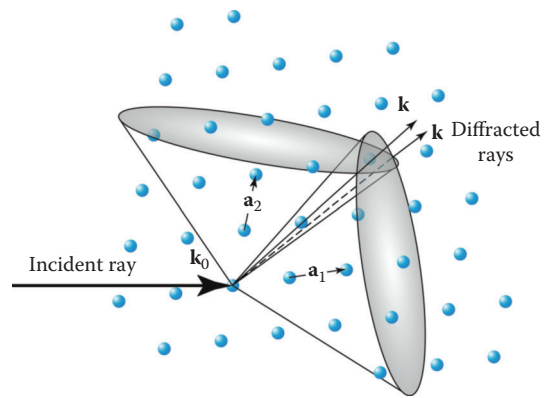
FIGURE 2.22

Max von Laue (1897–1960).

FIGURE 2.23

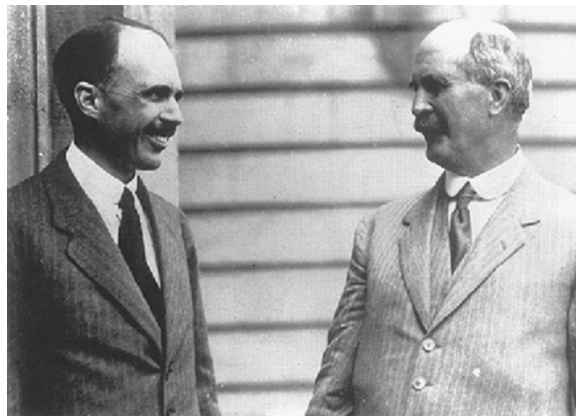Father and son Bragg: Sir William Henry and William Lawrence Bragg.

FIGURE 2.24

In case of mirror-like Bragg reflection, the vector $\Delta\mathbf{k}$, the summation of the unit vectors representing incoming ($\mathbf{k}_0$) and reflected rays ($\mathbf{k}$), is normal to the plane that intersects the 2θ angle between them. (Drawing by Mr. Chengwu Deng.)
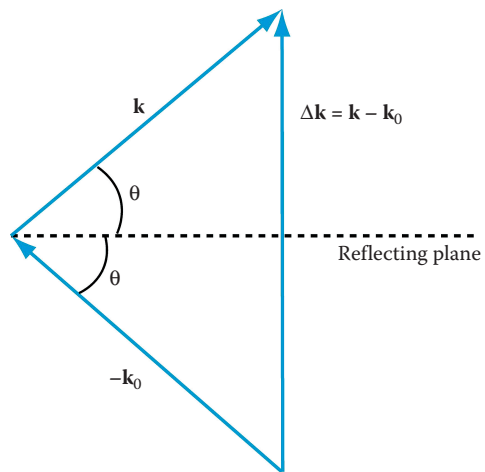
FIGURE 2.25

Connecting Bragg's law with Laue equations and Miller indices. (Drawing by Mr. Chengwu Deng.)
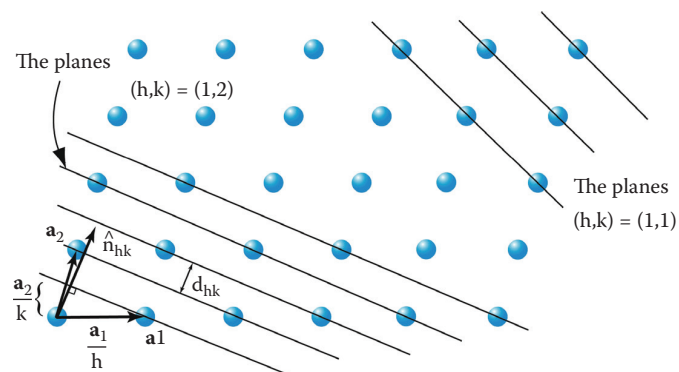
FIGURE 2.26

Sodium deoxyribose nucleate from calf thymus. (Structure B, Photo 51, taken by Rosalind E. Franklin and R.G. Gosling.) Linus Pauling's annotations are to the right of the photo (May 2, 1952).
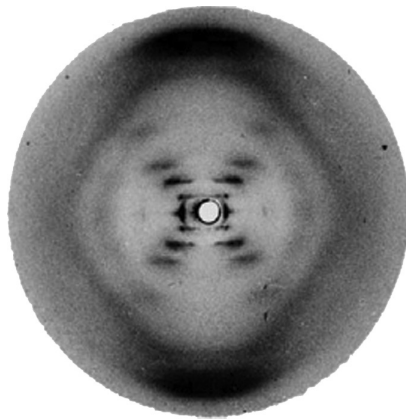
FIGURE 2.27

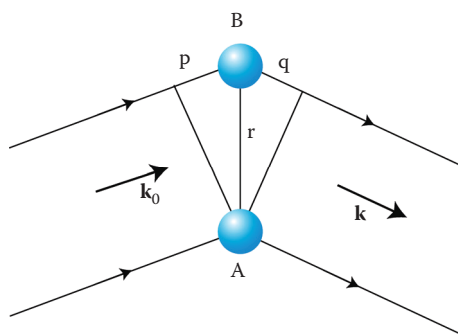Scattering of x-rays from two nearby atoms A and B with identical scattering density. (Drawing by Mr. Chengwu Deng.)

FIGURE 2.28

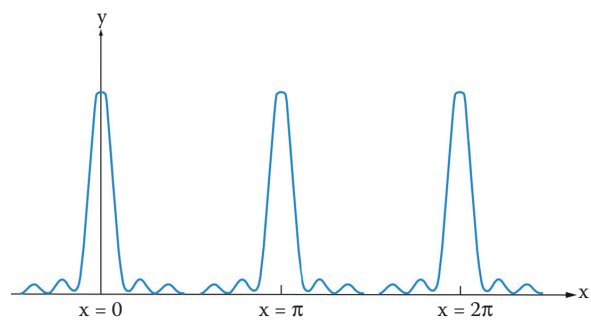Graphical presentation of $y = \sin^2 Mx/\sin^2 x$. The width of the peaks and the prominence of the ripples are inversely proportional to M.

FIGURE 2.29

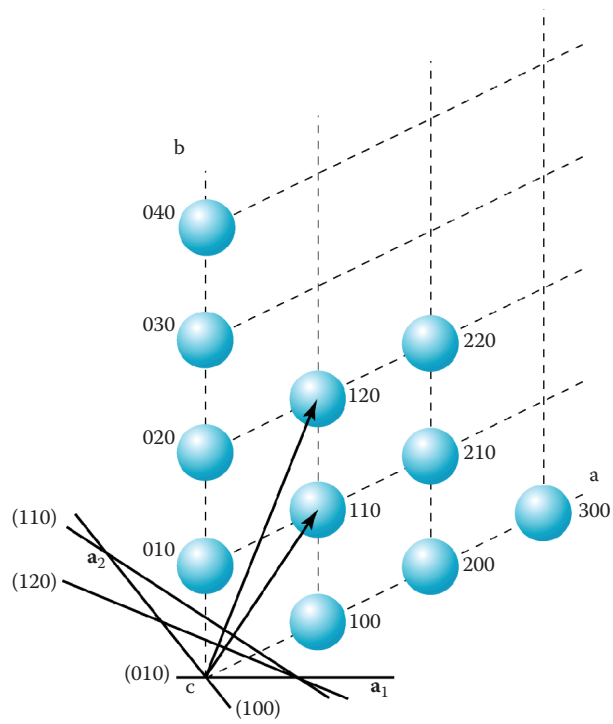Graphical construction of the reciprocal lattice. (Drawing by Mr. Chengwu Deng.)

FIGURE 2.30

Vector triangle representation of $\Delta\mathbf{k} = \mathbf{G}_{hkl}$. (Drawing by Mr. Chengwu Deng.)
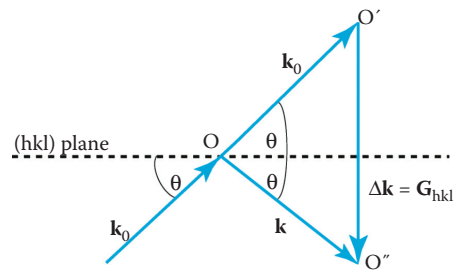
FIGURE 2.31

Reciprocal lattice vectors $a_1^* = G_{100}$ and $a_3^* = G_{001}$ in a monoclinic unit cell and their relation to the Bravais lattice. (Drawing by Mr. Chengwu Deng.)
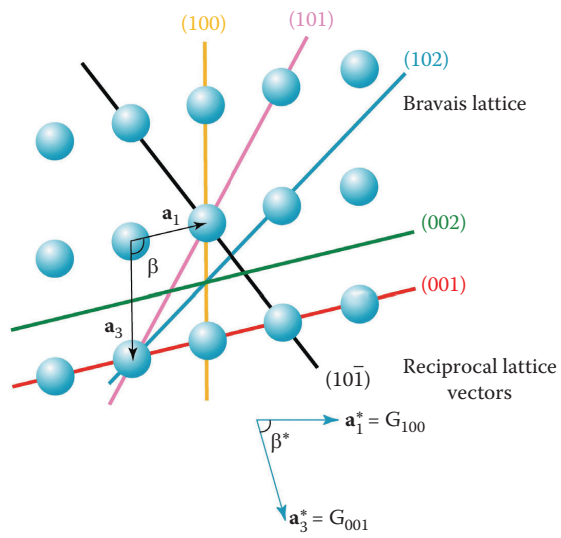
FIGURE 2.32

The reciprocal lattice and the geometry of diffraction clarified by the Ewald sphere. The sphere with center O intersects the reciprocal lattice center O'. (Drawing by Mr. Chengwu Deng.)
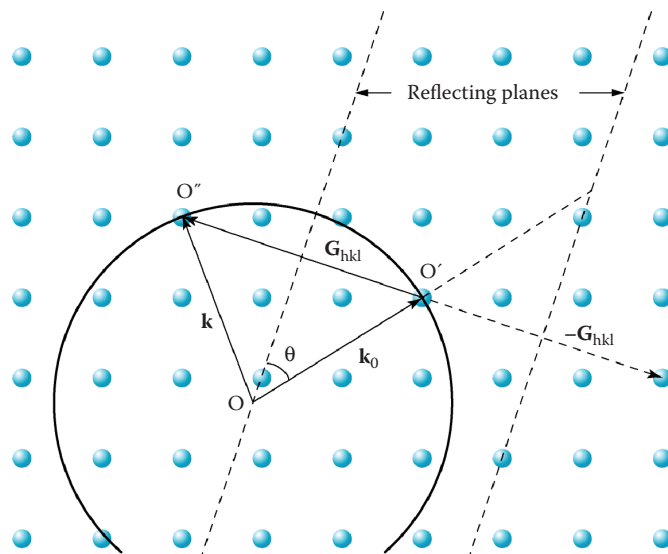
FIGURE 2.33

The Brillouin zones for (a) a square 2D lattice and (b) a triangular 2D lattice. The solid circles are the lattice points, and the dashed lines are the Bragg lines. The first four Brillouin zones are marked with different gray scales.
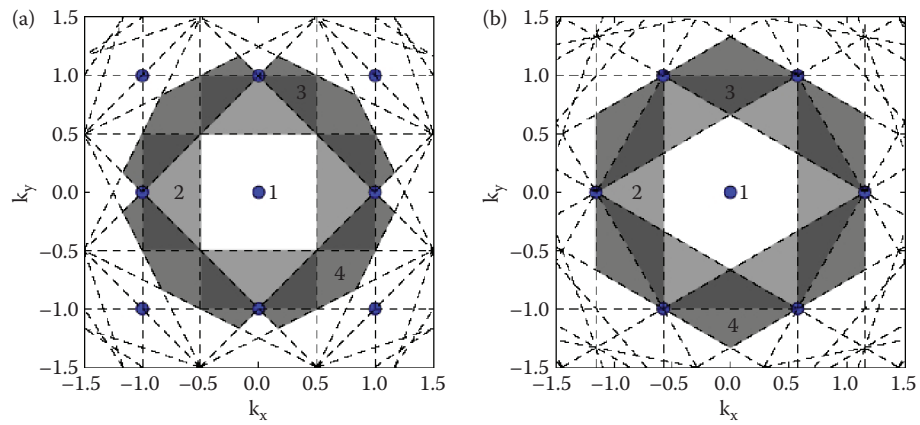
FIGURE 2.34

The Wigner-Seitz cell of BCC lattice in real space transforms to a Brillouin zone in an FCC lattice in reciprocal space, whereas the Wigner-Seitz cell of an FCC lattice transforms to a Brillouin zone of a BCC lattice in reciprocal space.
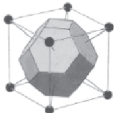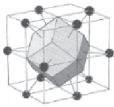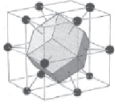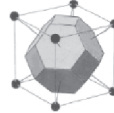

Lattice real space	Lattice **k**-space
BCC Wigner-Seitz cell	BCC BZ (FCC lattice in **k**-space)
FCC Wigner-Seitz cell	FCC BZ (BCC lattice in **k**-space)

FIGURE 2.35

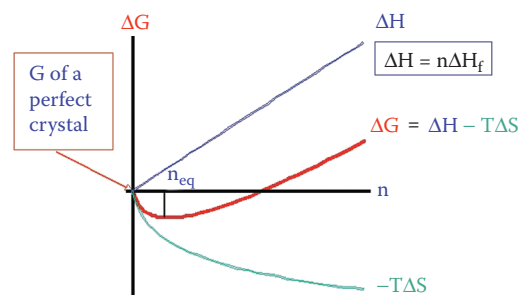Change in Gibbs free energy G of a crystal as a result of the number of vacancies n.

FIGURE 2.36

Point defects: vacancy (a), interstitial atom (b), small (c) and large (d) substitutional atom, Frenkel (e), and Schottky defect (f).

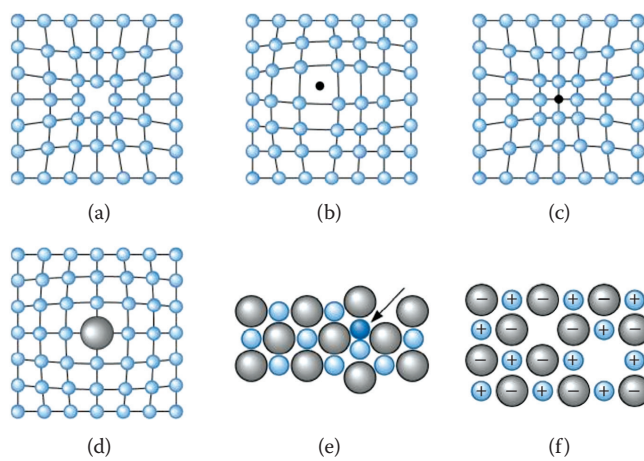(a)

(b)

(c)

(d)

(e)

(f)

FIGURE 2.37

Color centers in some well-known minerals: (a) the Dresden green diamond, (b) smoky quartz, and (c) amethyst or violet quartz.

(a) (b) (c)

FIGURE 2.38

(A) Edge dislocation: The perfect crystal in (a) is cut, and an extra plane of atoms is inserted (b). The bottom edge of the extra plane is an edge dislocation (c). A Burgers vector **b** is required to close a loop of equal atom spacings around the edge dislocation. (B) Screw dislocation: The perfect crystal (a) is cut and sheared over one atom spacing (b and c). The line along which shearing occurs is a screw dislocation. (C) A mixed dislocation: The screw dislocation at the front face of the crystal gradually changes to an edge dislocation at the side of the crystal.
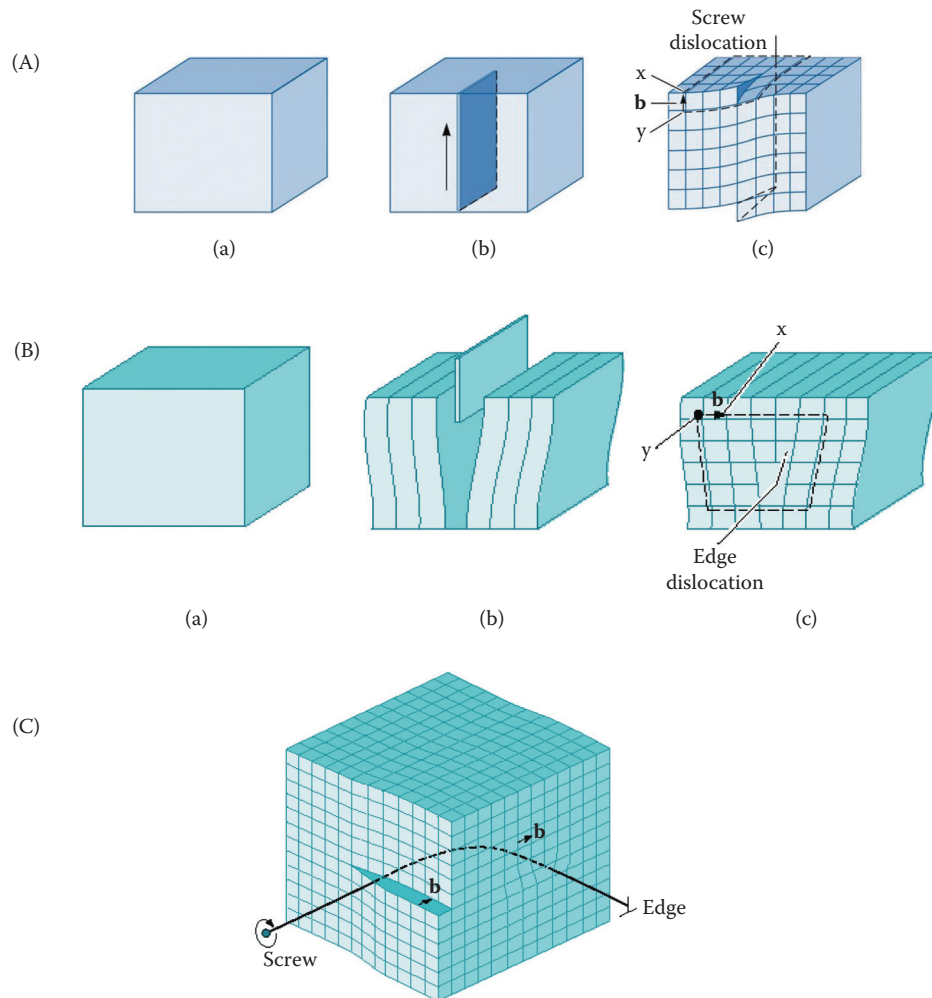
FIGURE 2.39

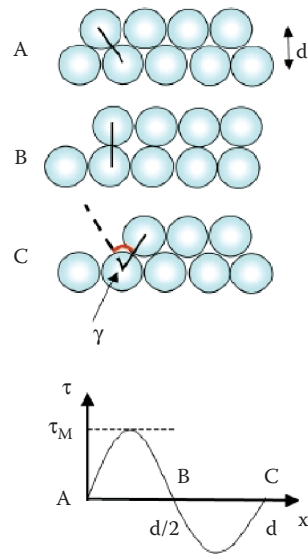Calculation of the theoretical shear stress in a crystal.

FIGURE 2.40

Shear stress, τ; shear strain, γ; and shear modulus, μ. The shear stress τ produces a displacement Δx of the upper plane as indicated; the shear strain, γ, with $\Delta x/d = \tan \alpha$ is defined $\gamma = \tau/\mu$.
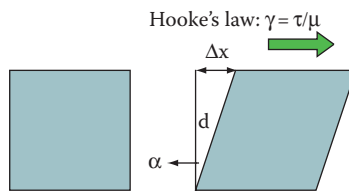
FIGURE 2.41

Dislocation movement: When a shear stress is applied to the dislocation in (a), the atoms are displaced, causing the dislocation to move one Burgers vector **b** in the slip direction (b). Continued movement of the dislocation eventually creates a step (c), and the crystal is deformed. (d) The caterpillar does not move its complete body at a single time, but it moves one segment at a time as it pulls itself forward.
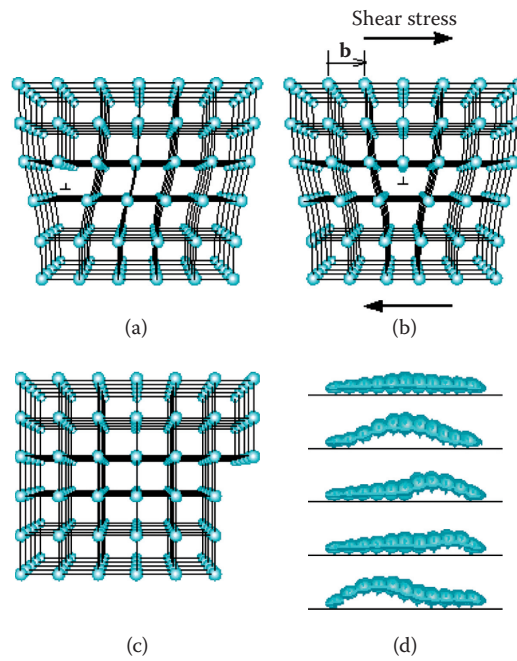
FIGURE 2.42

Moving a carpet over the floor to illustrate the effect of a line dislocation in a crystal: (a) dislocation; (b) work hardening.
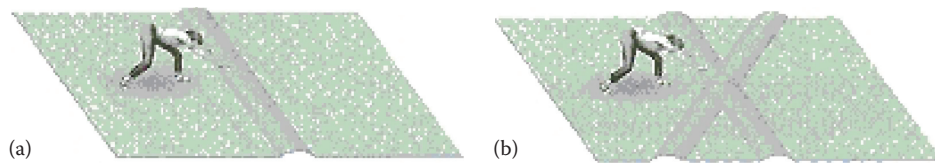

(a)

(b)

FIGURE 2.43

An applied shear stress, τ, exerts a force on a dislocation and is resisted by a frictional force, **F**, per unit length. The slip vector or Burgers vector is **b**. (Drawing by Mr. Chengwu Deng.)

FIGURE 2.44
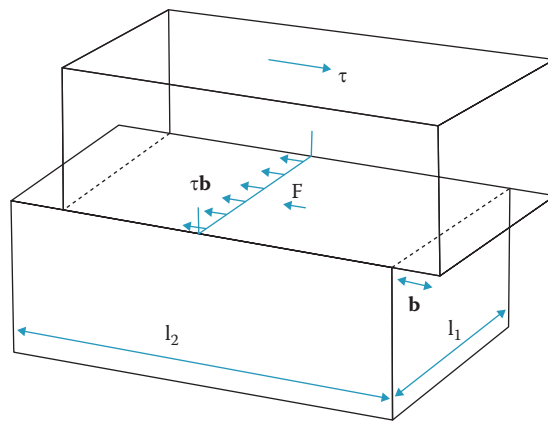
Schematic of slip line, slip plane, and slip (Burgers) vector for (a) an edge dislocation and (b) for a screw dislocation. (Drawing by Mr. Chengwu Deng.)
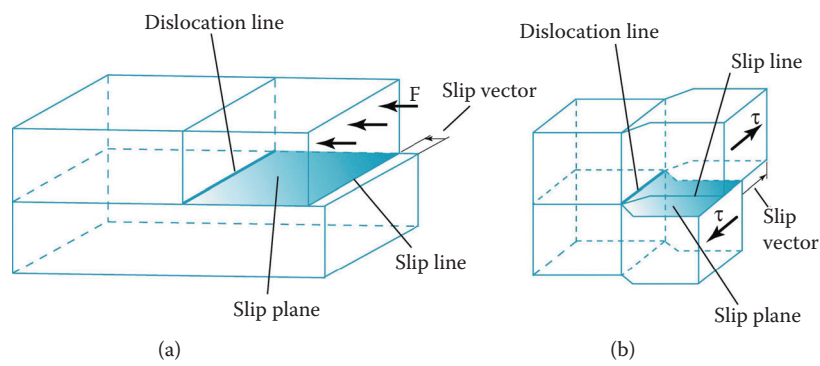

(a)

(b)

FIGURE 2.45

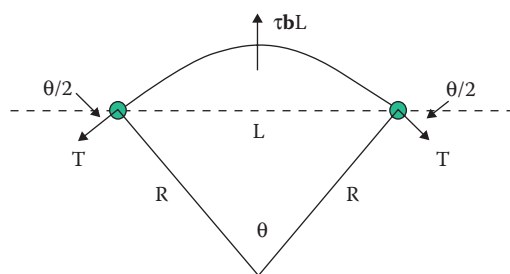A pinned dislocation bows under a shear stress.

FIGURE 2.46

A Frank-Read source can generate dislocations. (a) A dislocation is pinned at its ends by lattice defects. (b) As the dislocation continues to move, the dislocation bows, eventually bending back on itself. (c) Finally the dislocation loop forms, and (d) a new dislocation is created. (e) Electron micrograph of a Frank-Read source (×330,000).
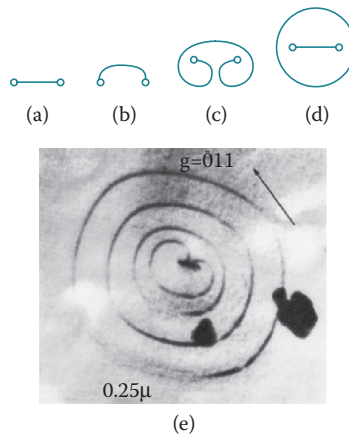
(a)   (b)   (c)   (d)

g=011

0.25µ

(e)

FIGURE 2.47

Geometry of slip plane, slip direction, and tensile force F. (Drawing by Mr. Chengwu Deng.)
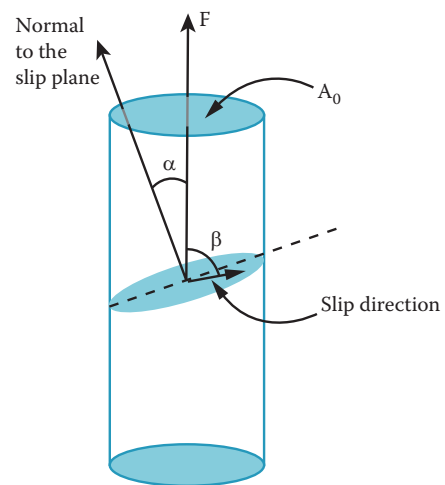
FIGURE 2.48

Crystal structure is disturbed at grain boundaries. Schematic representation of grain boundaries (a) and microscope picture (b). (From Askeland D. R., and P. P. Phule, *The science and engineering of materials*, Brooks/Cole, Pacific Grove, CA, 2003.)
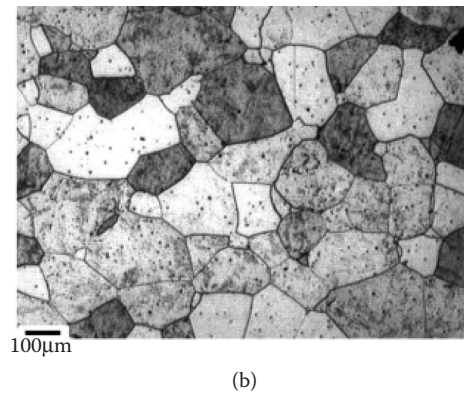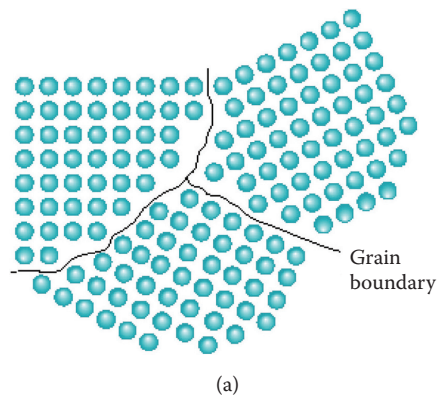

(a)

100μm

(b)

FIGURE 2.49

Nanoparticles, clusters of atoms in shells.
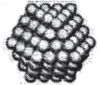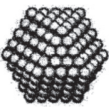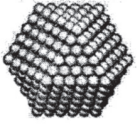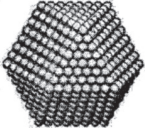
Full-Shell Clusters		Total Number of Atoms	Surface Atoms (%)
1 Shell		13	92
2 Shells		55	76
3 Shells		147	63
4 Shells		309	52
5 Shells		561	45
7 Shells		1415	35

FIGURE 2.50

SEM of a zinc whisker; diameter is 10 µm.